THE JOURNAL OF PHYSICAL CHEMISTRY C
A JOURNAL OF THE AMERICAN CHEMICAL SOCIETY

pubs.acs.org/JPCC

Article

High Harmonic Generation from 2D Polar Metal Heterostructures

Published as part of The Journal of Physical Chemistry C special issue "Naomi Halas and Peter Nordlander Festschrift".

Claudio Ordonez, Chengye Dong, Arpit Jain, Li-Syuan Lu, Joshua A. Robinson, and Kenneth L. Knappenberger, Jr.*

Cite This: *J. Phys. Chem. C* 2025, 129, 5133−5139

Read Online

ACCESS | Metrics & More | Article Recommendations | Supporting Information

ABSTRACT: High harmonic generation (HHG) from 2D polar metal heterostructures (PMets) is described. 2D Ag and Ga PMets were formed by confinement heteroepitaxy. High-temperature sublimation of Si atoms from 6H-SiC formed epitaxial bilayer graphene/SiC heterostructures (EG). Metal intercalation generated crystalline films of monolayer Ag and bilayer Ga in the confines of the graphene and SiC interface, forming the PMet heterostructure. HHG using a mid-infrared (5200 nm) laser to transduce the fifth, seventh, and ninth harmonics for both Ag and Ga PMets as well as EG exhibited a second-order dependence on the incident laser power. The quadratic power dependence implicated nonperturbative HHG mechanisms transduced by the graphene component of the heterostructures. The HHG signal intensity and polarization properties were sensitive to the choice of metal intercalant and, in the case of EG, the SiC support. This sensitivity resulted from metal- and SiC-to-graphene charge transfer (i.e., n-doping of graphene). The doping effect created a carrier population in the graphene conduction band, which resulted in an effective Pauli blocking that modulated the HHG response. The results show the potential for using multicomponent heterostructures for tailoring the frequency and polarization properties of photonic materials as well as the effectiveness of HHG for probing interfacial energy transfer.

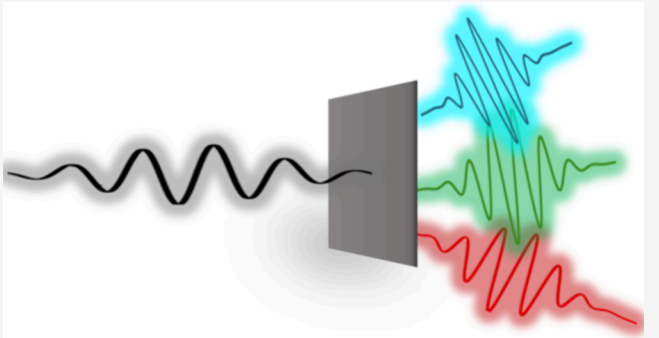

Downloaded via PENNSYLVANIA STATE UNIV on April 16, 2025 at 13:41:07 (UTC).
See https://pubs.acs.org/sharingguidelines for options on how to legitimately share published articles.

INTRODUCTION

Owing to their growth mechanism, 2D polar metal heterostructures (PMets), which feature few-atomic-layer crystalline metals, are rich with otherwise inaccessible metal lattice structures and compositions.[1−7] Grown through confinement heteroepitaxy, the 2D-PMet consists of three structural components: a 6H-silicon carbide substrate; a few atomic layers of crystalline metal; and bilayer graphene that caps the heterostructure. Because the 2D metal is capped with a graphene bilayer, the material is protected against oxidation and long-term (>9 months) storage under ambient conditions without degradation of the intercalated metal layers is possible.[1] Because the metals crystallize in the confines between epitaxial graphene and unpassivated silicon carbide, they are exposed to nonterminated SiC dangling bonds, which act as growth-facilitating, high-energy surfaces. The SiC template dictates the metal lattice structure, giving rise to a wide range of electronic, magnetic, catalytic, and photonic properties.[8]

When group III metals such as indium and gallium comprise the intercalated metal layer of the PMets, these metals adopt the hexagonal lattice registry of the 6H-SiC substrate. Cross-sectional STEM studies indicate that the change in interlayer lattice spacing across the layers of 2D Ga is approximately 10%,[2] which equates to a change in metal−metal bond length of approximately 200 picometers over three metal layers. According to first-principles calculations, the out-of-plane strain should be accompanied by an evolution in bonding character. While the bonding at the SiC-metal interface is predominately covalent, the bonding becomes metallic in the metal layers and is dominated by van der Waals interactions at the metal−graphene interface. The out-of-plane structure breaks the structure's centrosymmetry, creating an out-of-plane electrostatic dipole and allowing PMets to exhibit exceptionally large second-order nonlinear responses. In particular, second-order nonlinear susceptibilities $\chi^{(2)}$ of 4.6 ± 0.7 and 8.5 ± 0.6 nm/V for 2-D Ga and In, respectively, were determined from second harmonic generation micros-

Received: December 29, 2024
Revised: February 11, 2025
Accepted: February 13, 2025
Published: February 26, 2025

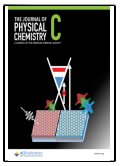

ACS Publications

© 2025 American Chemical Society

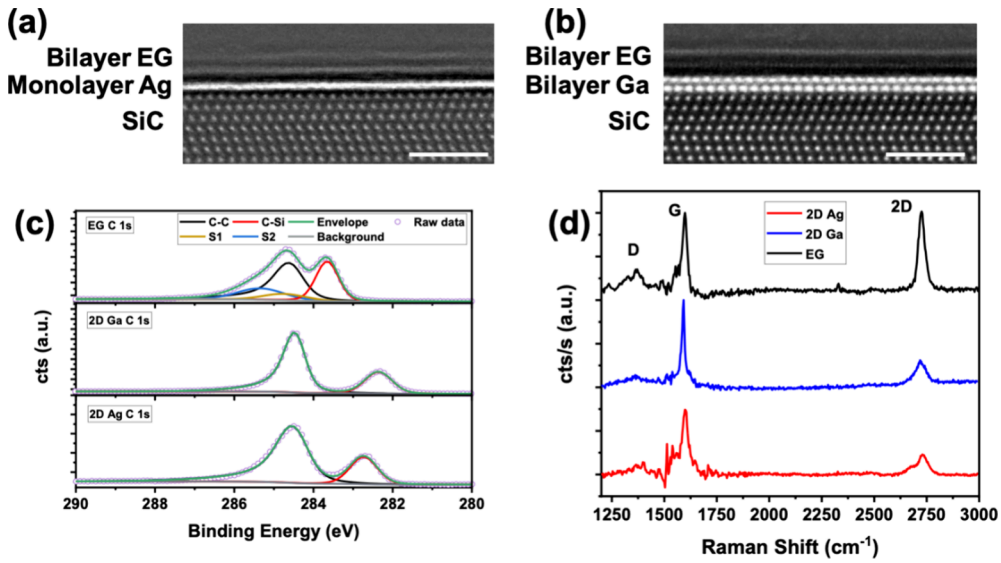

Figure 1. (a) Cross-sectional scanning transmission electron microscope images of (a) 2D-Ag and (b) 2D-Ga PMets. The images show the silicon carbide (SiC) lattice, mono- and bilayer Ag and Ga, respectively, and bilayer graphene. The scale bars are 2 nm in both (a) and (b). (c) X-ray photoelectron spectra of EG, 2D-Ga and 2D-Ag showing the disappearance of the 285 eV peak upon metal intercalation. (d) Raman spectra for EG (black), 2D Ga (blue) and 2D Ag (red) showing the decreasing G/2D ratio upon intercalation. The HHG was generated by a nonperturbative mechanism.

copy.[2] These experimentally determined per-volume $\chi^{(2)}$ values represent a more than 100-fold improvement over industrial standard $LiNbO_3$ and reflect the potential of PMets as photonic materials.

The choice of metal intercalant also affects energy dissipation for 2D-PMets.[9] The metal films are generally semiconducting, with a range of electronic bandgap energies.[8,10] Nearly degenerate transient absorption (TA) spectroscopy resolves three characteristic time scales for carrier relaxation: sub-1 ps, 15 ps, and a longer component, which persists beyond the 150 ps window of the measurement.[9] Electron−electron scattering likely occurs within the ∼300 fs instrument-response time, followed by subpicosecond electron−phonon coupling (t_1). The longer decay components (t_2 and t_3) are assigned to heat dissipation into the SiC lattice, with contributions from both the interfacial thermal conductivity and heat diffusion in the substrate. Time constants for these processes are dependent on the identity of the metal intercalant as well as alloy compositions of the metal. Therefore, the few-atomic-layer metal can play a substantial role in dictating energy-transfer efficiency in these materials. Although the TA data reflect transient processes monitored through the heterostructure's metal component, photoexcitation likely creates nonequilibrium carriers in both the metal and the graphene portions of the PMet. Thus, it is difficult to distinguish the influences of specific structural components on the electron dynamics of the heterostructure using solely TA-based measurements.

High harmonic generation (HHG) has recently emerged as a new frontier in solid-state materials research.[11] In contrast to the perturbative second harmonic generation (SHG) measurements described above for PMets, HHG is a nonperturbative strong-field process that transduces harmonics over a large energy range. In the gas-phase, HHG provides the basis for generating ultrafast laser pulses in the extreme ultraviolet and X-ray regions, including pulses with attosecond duration.[12−14] In the condensed phase, both the material lattice and electronic structures impact the HHG process, resulting in system-specific polarization properties, incident power dependences, and transduced photon orders.[15−22] In particular, graphene shows a unique HHG response that includes the generation of elliptical odd-order harmonics, which can be easily distinguished from signals arising from most semiconducting materials. Hence, HHG may provide an effective method for understanding carrier population and dynamics in PMets and other heterostructures.

Here, HHG from Ga- and Ag-intercalated PMets are compared to those from epitaxial graphene/SiC. The results indicate that HHG by these systems using 5200 nm fundamental were transduced by graphene and that the metal intercalant doped the graphene by charge-transfer processes.

EXPERIMENTAL SECTION

High Harmonic Generation Spectroscopy. High harmonics were generated using a mid-infrared (MIR) laser pulse that served as the fundamental. The MIR pulse was produced using a difference-frequency mixing of signal and idler outputs from an 800 nm pumped optical parametric amplifier (OPA). The OPA was seeded by a regeneratively amplified Ti:sapphire laser operating at 1 kHz. The MIR carrier energy (wavelength) was centered at 0.24 eV (5200 nm). Mid-infrared pulses were focused onto the sample with a ZnSe aspheric focusing lens (NA = 1.24). HH were collected in a transmission geometry microscope with a 4x objective, which focused the emission radiation onto the spectrometer entrance slit. The ellipticity of the MIR pulse was controlled using a $\lambda/4$-wave plate, while the major axis is controlled using a $\lambda/2$-wave plate. The emission polarization was selected using a CaF_2 wire grid polarizer that served as an analyzer to isolate the E_x and E_y components of the high harmonic signals. To record the spectral information, a spectrometer (Teledyne Princeton Instruments) and charge-coupled device camera (BLAZE, Teledyne Princeton Instruments) were used.

https://doi.org/10.1021/acs.jpcc.4c08773
J. Phys. Chem. C 2025, 129, 5133−5139

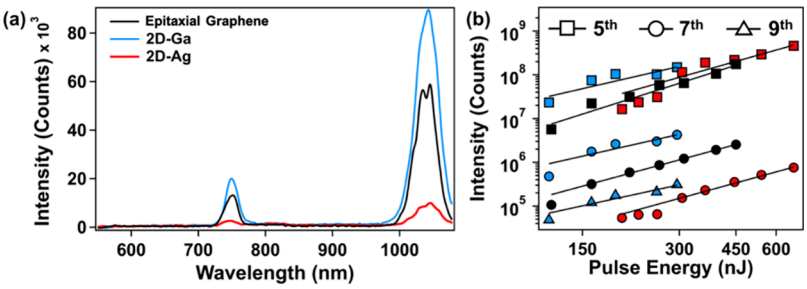

Figure 2. (a) High harmonic generation (HHG) spectra from 2D Ag (blue) and 2D Ga (red) polar metals (PMets) and epitaxial graphene (EG) using a 200-nJ pulse. The spectra show the 5th (1040 nm) and 7th (745 nm) harmonic signals from each sample. (b) HHG intensity ($I_{n\omega}$) plotted as a function of fundamental power ($P_{1\omega}{}^n$). The data follow the power-law function, $I_{n\omega} = P_{1\omega}{}^n$, where n is the fundamental photon order. For each harmonic, n ≈ 2 was obtained, indicating the HHG was generated by a nonperturbative mechanism.

Synthesis of Epitaxial Graphene and 2D Polar Metals. EG was prepared on the (0001) plane of semi-insulating 6H-SiC (Coherent corp.) via silicon sublimation. Clean SiC substrate was first annealed at 1400 °C, 700 Torr in 10% H_2/Ar mixture for 30 min to remove residues on the surface. Then it was annealed at 1800 °C, 700 Torr in pure Ar for 20 min to synthesize monolayer EG.

EG was plasma-treated using a Tepla M4L plasma etch tool with 150 sccm O_2 and 50 sccm He at 500 mTorr pressure, 50 W power, for 60 s to create defects for metal intercalation. Two-dimensional silver and gallium intercalation was performed in a Thermo Scientific Lindberg/Blue M Mini-Mite tube furnace. An alumina crucible (Robocasting Enterprises) held 1 × 0.5 cm2 EG/SiC substrates with the EG/Si face downward. Ag powder (85 mg, Sigma-Aldrich, 99.999%) or Ga powder (50 mg, Sigma-Aldrich, 99.999%) was placed beneath the substrate inside the crucible for 2D Ag and Ga synthesis, respectively. The assembly was pressurized to 500 Torr with 50 sccm Ar, heated to 900 °C at a 50 °C/min ramp rate, and maintained at 900 °C for 1 h, then cooled to room temperature for synthesizing 2D Ag. 2D Ga was prepared at 800 °C, 500 Torr with 50 sccm Ar for 30 min.

RESULTS AND DISCUSSION

High harmonic generation was studied for three different 2D materials platforms: 1) epitaxial graphene (EG); 2) 2D-Ga PMets; and 3) 2D-Ag PMets. EG was synthesized by sublimation of silicon from the 0001 plane of 6H-SiC. EG formation was confirmed by X-ray photoelectron and Raman scattering spectroscopy measurements. EG includes a graphene buffer layer that partially passivates the supporting SiC surface. The buffer layer exhibits a distinct XPS peak at approximately 285 eV binding energy as well as characteristic Raman scattering peaks at 2700 cm^{-1} (so-called 2D peak) and 1600 cm^{-1} (G peak).[23] Metals readily intercalate at the EG/SiC interface, forming 2D crystalline metal films epitaxial to the 6H-SiC template. A representative example of the metals studied here is shown in the cross-sectional scanning tunneling electron microscope image in Figure 1. Further evidence of metal intercalation is obtained from the disappearance of the 285-eV XPS peak and an increase in the G/2D Raman intensity ratio; metal intercalation releases the EG buffer layer.

High Harmonic Generation spectra from 2D Ag- and Ga-intercalated polar metals and epitaxial graphene/silicon carbide (EG) are shown in Figure 2a. The plotted energy range portrays the fifth and seventh harmonics for each sample, and an intensity ordering of 2D-Ag < EG < 2D-Ga was observed. Graphene is known to transduce mid-infrared light to high-order odd harmonics by a nonperturbative mechanism.[19] However, to date, only perturbative second harmonic generation has been studied for 2D PMets.[2] To confirm whether the high-order harmonics from 2D PMets resulted from nonperturbative HHG or a perturbative mechanism, the dependence of the harmonic intensity ($I_{n\omega}$) on the mid-infrared laser power ($P_{1\omega}$) was analyzed using the power-law expression, $I_{n\omega} = P_{1\omega}{}^n$, where n is the photon order of the harmonic. These results are summarized in Figure 2b. In the case of perturbative harmonic generation, a direct correlation between the signal intensity and the fundamental photon order is expected; for example, second and third harmonic generation will be quadratic and cubic, respectively. In contrast, this scaling will not be observed for nonperturbative harmonic generation; rather, a saturated photon order intrinsic to the material results.[22] The intensities of the fifth, seventh, and ninth harmonics from Ga 2D-PMets (blue markers) are plotted versus fundamental power in Figure 2b. These signal intensities exhibited an n ≈ 2 power dependence, indicating the harmonics resulted from nonperturbative HHG. Similarly, the intensity of the fifth and seventh harmonics transduced by Ag 2D-PMets (red markers) are plotted versus fundamental power in Figure 2b; the ninth harmonic was not detected for this system. For both high-order signals, a photon order of n ≈ 2 was detected, confirming that all harmonics for both polar metal systems were generated by a nonperturbative mechanism. The fifth and seventh harmonics from EG (black markers) gave a value of n ≈ 2.1. These values are consistent with previous measurements of graphene on quartz, which gave a quadratic power dependence for the HHG yields.[19]

There are three significant observables from the Figure 2 data: 1) only odd-order harmonics are detected; 2) all samples show a common n ≈ 2 HHG power dependence; and 3) the HHG signal yield is sensitive to the identity of the metal intercalant. The implications of each of these three observations will be discussed in the remainder of this manuscript. For graphene on quartz, odd orders are transduced with a quadratic power dependence, and even-order HHG is not detected.[19] The detection of only odd-order harmonics is reconciled using a semimetal model for HHG,[24,25] which involves the linear dispersion and zero-energy gap of the Dirac cone that characterizes the graphene band structure.[26,27] In contrast, HHG from semiconducting systems with high-energy electronic bandgaps exhibit more complicated HHG spectra, which can include even-order harmonics.[17,18,20,22] These even-order signals generally occur when the material lattice breaks inversion symmetry. 2D polar metals break inversion symmetry at the metal-SiC interface.[2] Further, both Ga and Ag PMets are

https://doi.org/10.1021/acs.jpcc.4c08773
J. Phys. Chem. C 2025, 129, 5133−5139

semiconducting with electronic bandgaps in the near-infrared.[2,9,10] Hence, high harmonics from 2D metals can be expected to include even-order harmonic signals. Therefore, the HHG transduced by 2D PMets and EG using 5200 nm MIR is attributed to the graphene layer, and the intensity differences observed in Figure 2a are ascribed to graphene doping by the substrate. In order to verify this interpretation, the polarization-dependent HHG responses of the PMets and EG were studied.

HHG from graphene is mediated by both interband and intraband mechanisms. The interband model is qualitatively similar to the three-step model used to describe gas-phase HHG. The fundamental laser field causes electrons to tunnel to the conduction band. The resultant conduction band electrons and valence band holes are accelerated under the force exerted by the incident laser field and subsequently radiate high harmonics with energies determined by their respective k-space positions. Owing to the similarities between the interband and gas-phase three-step models, solid-state HHG yields resulting from interband processes are maximal for linearly polarized fundamental lasers and decrease as the driving field polarization is modulated. In contrast, intraband HHG is described as a superposition of high-order wave functions, and, as such, can take on phase-dependent properties. As a result of contributions from both interband and intraband mechanisms, graphene-transduced HHG is enhanced by elliptical fundamental driving fields.

Figure 3 compares the 2D-Ag seventh-harmonic signal intensities detected in orthogonal (x and y) directions as the

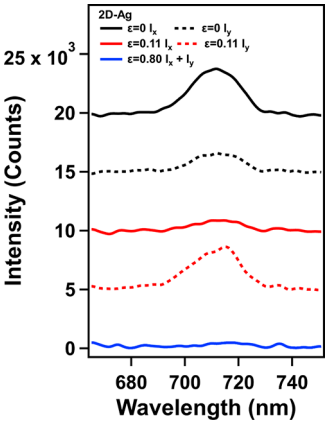

Figure 3. Seventh harmonic spectra from 2D Ag PMets detected in the x and y directions, generated using linear (ε = 0) and select elliptical (ε = 0.11 and ε = 0.80) MIR polarization states. Spectra were obtained using a 200-nJ MIR pulse.

MIR polarization is translated from linear to select elliptical polarization states. The MIR polarization state is expressed as $\varepsilon = I_y/I_x$, where I_y and I_x are laser intensities measured in the y- and x-laboratory planes; propagation is along the z axis. An ε value of zero corresponds to linearly polarized light oriented in the x direction, ε = 1 is circularly polarized, and any ε value between 0 and 1 represents an elliptical polarization state. Harmonic signal strengths detected in the x and y directions are denoted as H_x and H_y, respectively. The various polarization schemes are shown schematically in Figure 4a. HHG yields from atoms and high-energy-gap semiconductors are maximal when ε = 0, and they decrease monotonically when the polarization phase is adjusted away from a linear

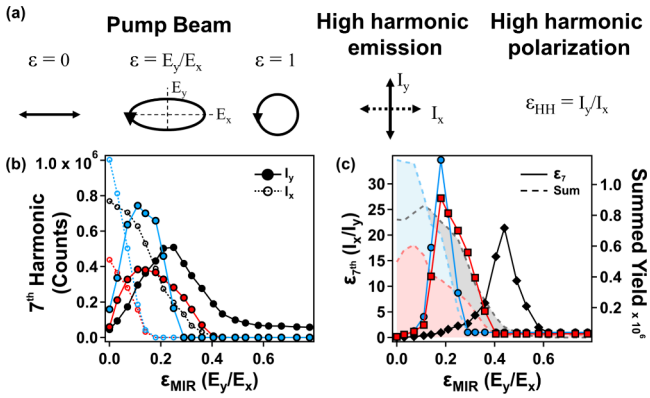

Figure 4. (a) Schematic describing the different polarization states used in the ellipticity measurements. (b) Seventh harmonic HHG intensity detected in the x (open circle) and y (filled circle) directions plotted as a function of fundamental ellipticity for 2D-Ag (red), 2D-Ga (blue) and EG (black) (c) Ellipticity of the seventh harmonic signal plotted as a function of fundamental ellipticity, adopting the same color coding as in panel (b).

state.[19,28] This is in contrast to what is observed for the Ag 2D-PMets (Figure 3). A linearly polarized (ε = 0) incident MIR fundamental transduces an elliptical seventh-harmonic response; the signal is a superposition of nonequivalent H_x and H_y components. Note that the majority of the HHG signal is x-polarized, but a significant H_y component is detected. Hence, HHG transduction by the PMet structure results in both frequency and polarization modulation. Upon using elliptical MIR (ε = 0.11), H_y signals dominate the HHG spectrum, with the H_x response substantially suppressed. It is notable that the dominant HHG signal is y-polarized even though the MIR polarization retains primary intensity from the I_x component. Further modulation of the MIR polarization state to ε = 0.8 suppressed all HHG signals. The polarization response depicted in Figure 3 is consistent with contributions from intraband HHG in addition to interband contributions.[17−19] Although Figure 3 depicts only 2D-Ag PMet data, qualitatively similar trends were obtained for 2D-Ga PMets and EG samples. A similar effect has also been observed for monolayer graphene on quartz.

Figure 4b compares the polarization dependencies of the seventh-harmonic signals from 2D-Ag (red) and 2D-Ga (blue) PMets and EG (black) using a continuous modulation of the MIR polarization from linear (ε = 0) to elliptical ($0 < \varepsilon < 1$) to circular (ε = 1) states. The seventh-harmonic response for ε = 0 from each sample shows an intense peak for I_x (open circle, dashed line) detection and a smaller, but non-negligible, I_y signal (closed circle, solid line). A continuous change in dominance from H_x to H_y signal is observed for all samples as the ellipticity is increased. For both 2D-Ag and 2D-Ga, the maximum H_y signal is detected when $\varepsilon \approx 0.15$. For EG, the maximum H_y signal is detected when $\varepsilon \approx 0.24$. The EG sample yields a polarization dependence similar to that of graphene on quartz, which also shows maximum H_y signal when $\varepsilon \approx 0.24$; this is attributed to large contributions from intraband HHG mechanisms.[19] Similar to the overall intensity yields described in Figure 2a, the intercalation of 2D crystalline metals into the EG system impacts the polarization modulation, resulting in maximal orthogonal signal transduction at lower values of MIR ellipticity. The ellipticity of the seventh-harmonic signal for each sample is compared versus MIR ellipticity in Figure 4c,

https://doi.org/10.1021/acs.jpcc.4c08773
J. Phys. Chem. C 2025, 129, 5133−5139

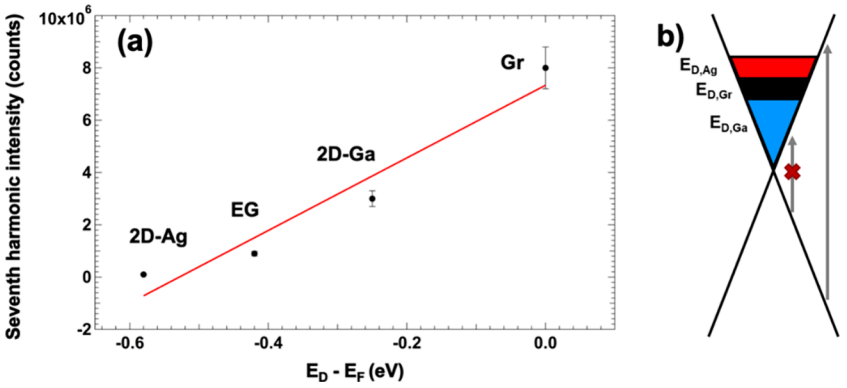

Figure 5. (a) Seventh harmonic integrated intensity from 2D-Ag and Ga PMets, epitaxial graphene (EG) and graphene on quartz (Gr), plotted as a function of the energy difference between the Dirac point and Fermi level energies ($E_D - E_F$). The energy values are obtained from previously published ARPES measurements.[10] The red line is a linear fit to the data. Data were acquired using a fundamental pulse energy of 250 nJ. (b) Schematic describing the influence of metal intercalation and SiC doping on graphene, which modifies carrier population in graphene conduction band states. Increased carrier population reduces the harmonic intensity, as shown in panel (a) and effects polarization modulation as shown in Figures 3 and 4. E_D-E_F values are adapted from [10]. Copyright 2022 American Chemical Society.

which tracks the Figure 4b data. The ellipticity data are notable because the results implicate the intraband mechanism as one component of the HHG signal for these samples. The intraband signal requires orthogonal applied fields for transduction, such as those present in an elliptical polarization state. Figure 4c also shows the total seventh-harmonic signal as a summed yield of $H_x + H_y$ (filled area under dashed line) for each sample. Significantly, for the 2D metals, these plots show maximum HHG signal is achieved at $0 < \varepsilon < 0.15$. Since the interband mechanism dominates at $\varepsilon = 0$,[17−19] the polarization results implicate a superposition of both interband and intraband mechanisms in the HHG process, with relative contributions varying as the MIR polarization state is modulated.

Taken together, the photon order ($n \propto 2$) and the HHG intensity polarization dependencies for the 2D-Ag, 2D-Ga, and EG samples are in excellent agreement with previous results on monolayer graphene.[19] Therefore, we attribute the HHG signals reported in Figures 2−4 to transduction by the graphene component of the PMet and EG systems. The quantitative differences in the polarization dependences and the metal-specific HHG signal strengths are attributed to influences of the metal on graphene, such as doping or changes in carrier density. In order to assess these influences, we have correlated the HHG intensities with angle-resolved photoelectron spectroscopy (ARPES) data (Figure 5a). Prior ARPES measurements on 2D PMets show that certain metals n-dope graphene, resulting in a shift of the Dirac point to an energy lower than the Fermi level.[10] A similar effect occurs in EG, with respect to free-standing monolayer graphene, because of charge transfer from the SiC surface to graphene. The HHG integrated intensity (7th harmonic) is plotted versus the energy difference between the Dirac point and Fermi level energies for each sample, including graphene on quartz, in Figure 5a. A clear correlation between the HHG intensity and the E_D-E_F values was observed. This direct correlation between the energy dependence and the harmonic intensity is best illustrated by a linear (red line) fit to the HHG data. A similar trend was observed for the fifth harmonic signals (Figure S1). We note that this fit is phenomenological and rigorous models should be developed to reconcile the intensity vs energy scaling.

A generalized scheme that reconciles the MIR power and polarization-dependent responses as well as the intercalant specificity is given in Figure 5b. HHG in all samples occurs from nonperturbative processes mediated by graphene. Metal intercalation and SiC serve to n-dope the graphene layer, lowering the Dirac point and creating increased carrier population in conduction-band states. This population causes an effective Pauli blocking that systematically reduces the interband HHG yield with respect to that of free-standing graphene. The observed modulation of the ellipticity response can also be understood from reduced interband contributions to the HHG signal; the H_y signal component is derived from the intraband mechanism. We note that the trend in the ellipticity data is not as direct as the clear correlation between HHG intensity and $E_D - E_F$ values due to doping, and future experimental and theoretical studies will be helpful to develop a complete understanding of the polarization dependence. In summary, the results show that metal intercalation and graphene doping are effective approaches to modulate the intensity and polarization response of graphene-transduced HHG. These data also demonstrate the utility of HHG measurements for studying interfacial charge transfer in multicomponent systems.

CONCLUSIONS

High harmonic generation from 2D gallium and silver PMets and epitaxial graphene/SiC are reported. For each system, the intensity of the fifth and seventh harmonics exhibited a quadratic dependence on the 5200 nm laser fundamental, implicating a nonperturbative harmonic generation mechanism. The ninth harmonic, detected for 2D-Ga PMets, also showed a quadratic response. Importantly, elliptical harmonic signals as well as an ellipticity dependence on the fundamental laser polarization state were detected; these are signatures of HHG transduced by graphene. The harmonics showed contributions from both graphene interband and intraband tunneling mechanisms. The HHG signals indicated a metal-specific intensity response, which was correlated with a lowering of the Dirac point energy level. Reduction of the Dirac point energy allowed for metal and SiC charge transfer to graphene. This charge-transfer process resulted in the population of graphene conduction-band states, which caused

https://doi.org/10.1021/acs.jpcc.4c08773
J. Phys. Chem. C 2025, 129, 5133−5139

an effective Pauli blocking that reduced the HHG signal intensities transduced by the graphene component of the heterostructure. The results show that HHG may become a powerful tool for understanding component-specific influences on the electronic properties and carrier dynamics of multicomponent systems. The 2D metals may provide advantages for controlling energy transfer at interfaces and for expanding photonic applications of solid-state materials over a broad frequency range.

■ ASSOCIATED CONTENT

Supporting Information

The Supporting Information is available free of charge at https://pubs.acs.org/doi/10.1021/acs.jpcc.4c08773.

Supporting Information includes HHG data (PDF)

■ AUTHOR INFORMATION

Corresponding Author

Kenneth L. Knappenberger, Jr. − *Department of Chemistry, Pennsylvania State University, University Park, Pennsylvania 16802, United States;* orcid.org/0000-0003-4123-3663; Email: klk260@psu.edu

Authors

Claudio Ordonez − *Department of Chemistry, Pennsylvania State University, University Park, Pennsylvania 16802, United States*

Chengye Dong − *Department of Materials Science and Engineering and Two-dimensional Crystal Consortium, Materials Research Institute, Pennsylvania State University, University Park, Pennsylvania 16802, United States*

Arpit Jain − *Department of Materials Science and Engineering, Pennsylvania State University, University Park, Pennsylvania 16802, United States*

Li-Syuan Lu − *Department of Materials Science and Engineering, Pennsylvania State University, University Park, Pennsylvania 16802, United States*

Joshua A. Robinson − *Department of Materials Science and Engineering and Two-dimensional Crystal Consortium, Materials Research Institute, Pennsylvania State University, University Park, Pennsylvania 16802, United States;* orcid.org/0000-0002-1513-7187

Complete contact information is available at: https://pubs.acs.org/10.1021/acs.jpcc.4c08773

Author Contributions

The manuscript was written through contributions of all authors. All authors have given approval to the final version of the manuscript.

Notes

The authors declare no competing financial interest.

■ ACKNOWLEDGMENTS

This work was supported by a grant from the Air Force Office of Scientific Research, grant number FA9550-22-1-0402. A portion of this work was supported by the National Science Foundations, award number (DMR-2011839 and DMR-1539916). We thank Dr. Jane A. Knappenberger for careful reading of the manuscript.

■ REFERENCES

(1) Briggs, N.; Bersch, B.; Wang, Y.; Jiang, J.; Koch, R. J.; Nayir, N.; Wang, K.; Kolmer, M.; Ko, W.; Duran, A. D. L. F.; et al. Atomically Thin, Half-van Der Waals Metals Enabled by Confinement Heteroepitaxy. *Nat. Mater.* **2020**, *19*, 637−643.

(2) Steves, M. A.; Wang, Y.; Briggs, N.; Zhao, T.; El-Sherif, H.; Bersch, B. M.; Subramanian, S.; Dong, C.; Bowen, T.; Duran, A. D. L. F; et al. Unexpected Near-Infrared to Visible Nonlinear Optical Properties from 2-D Polar Metals. *Nano Lett.* **2020**, *20* (11), 8312−8318.

(3) Manjavacas, A.; García de Abajo, F. J. Tunable Plasmons in Atomically Thin Gold Nanodisks. *Nat. Commun.* **2014**, *5* (1), 3548.

(4) Sundararaman, R.; Christensen, T.; Ping, Y.; Rivera, N.; Joannopoulos, J. D.; Soljačić, M.; Narang, P. Plasmonics in Argentene. *Phys. Rev. Mater.* **2020**, *4* (7), No. 074011.

(5) Liao, M.; Zang, Y.; Guan, Z.; Li, H.; Gong, Y.; Zhu, K.; Hu, X. P.; Zhang, D.; Xu, Y.; Wang, Y. Y.; et al. Superconductivity in Few-Layer Stanene. *Nat. Phys.* **2018**, *14* (4), 344−348.

(6) Briggs, N.; Gebeyehu, Z. M.; Vera, A.; Zhao, T.; Wang, K.; De La Fuente Duran, A.; Bersch, B.; Bowen, T.; Knappenberger, K. L., Jr; Robinson, J. A. Epitaxial graphene/silicon carbide intercalation: a minireview on graphene modulation and unique 2D materials. *Nanoscale* **2019**, *11*, 15440−15447.

(7) Nisi, K.; Subramanian, S.; He, W.; Ulman, K. A.; El-Sherif, H.; Sigger, F.; Lassaunière, M.; Wetherington, M. T.; Briggs, N.; Gray, J.; et al. Light−Matter Interaction in Quantum Confined 2D Polar Metals. *Adv. Funct. Mater.* **2021**, *31* (4), No. 2005977.

(8) Lin, Y.; Torsi, R.; Younas, R.; Hinkle, C. L.; Rigosi, A. F.; et al. Recent Advances in 2D Material Theory, Synthesis, Properties, and Applications. *ACS Nano* **2023**, *17*, 9694−9747.

(9) Steves, M. A.; Rajabpour, S.; Wang, K.; Dong, C.; He, W.; Quek, S. Y.; Robinson, J. A.; Knappenberger, K. L., Jr. Atomic-Level Structure Determines Electron-Phonon Scattering Rates in 2-D Polar Metal Heterostructures. *ACS Nano* **2021**, *15*, 17780−17789.

(10) Lee, W.; Wang, Y.; Qin, W.; Kim, H.; Liu, M.; Nunley, N. T.; Fang, B.; Maniyara, R.; Dong, C.; Robinson, J. A.; et al. Confined Monolayer Ag as a Large Gap Semiconductor and Its Momentum Resolved Excited States. *Nano Lett.* **2022**, *22*, 7841−7847.

(11) Ghimire, S.; DiChiara, A. D.; Sistrunk, E.; Agostini, P.; DiMauro, L. F.; Reis, D. A. Observation of high-order harmonic generation in a bulk crystal. *Nat. Phys.* **2011**, *7*, 138−141.

(12) Ferray, M.; L'Huillier, A.; Li, X. F.; Lompre, L. A.; Mainfray, G.; Manus, C. Multiple-harmonic conversion from 1064 nm radiation in rare gases. *J. Phys. B. At. Mol. Opt. Phys.* **1988**, *21*, L31.

(13) Nugent-Glandorf, L.; Scheer, M.; Samuels, D. A.; Bierbaum, V. M.; Leone, S. R. Ultrafast photodissociation of Br2: Laser-generated high-harmonic soft x-ray probing of the transient photoelectron spectra and ionization cross sections. *J. Chem. Phys.* **2002**, *117*, 6108−6116.

(14) Corkum, P. B.; Krausz, F. Attosecond Science. *Nat. Phys.* **2007**, *3*, 381−387.

(15) Langer, F.; Hohenleutner, M.; Schmid, C. P.; Poellmann, C.; Nagler, P.; Korn, T.; Sherwin, M. S.; Huttner, U.; Steiner, J. T.; et al. Lightwave-driven quasiparticle collisions on a subcycle timescale. *Nature* **2016**, *533*, 225−229.

(16) Ndabashimiye, G.; Ghimire, S.; Wu, M.; Browne, D. A.; Schafer, K. J.; Gaarde, M. B.; Reis, D. A. Solid-state harmonics beyond the atomic limit. *Nature* **2016**, *534*, 520−523.

(17) Liu, H.; Li, Y.; You, Y. S.; Ghimrie, S.; Heinz, T. F.; Reis, D. A. High-harmonic generation from an atomically thin semiconductor. *Nat. Phys.* **2016**, *13*, 262−265.

(18) You, Y. S.; Reis, D. A.; Ghimire, S. Anisotropic high-harmonic generation in bulk crystals. *Nat. Phys.* **2017**, *13*, 345−349.

(19) Yoshikawa, N.; Tamaya, T.; Tanaka, K. High-harmonic generation in graphene enhanced by elliptically polarized light excitation. *Science* **2017**, *356*, 736−738.

(20) Jiang, S.; Chen, J.; Wei, H.; Yu, C.; Lu, R.; Lin, C. D. Role of the Transition Dipole Amplitude and Phase on the Generation of

Odd and Even High-Order Harmonics in Crystals. *Phys. Rev. Lett.* **2018**, *120*, No. 253201.
(21) Kovalev, S.; Dantas, R. M. A.; Germanskiy, S.; Deinert, J. C.; Green, B.; Ilyakov, I.; Awari, N.; Chen, M.; Bawatna, M.; Ling, J.; Xiu, F.; van Loosdrecht, P. H. M.; Surówka, P.; Oka, T.; Wang, Z. Non-perturbative terahertz high-harmonic generation in the three-dimensional Dirac semimetal Cd_3As_2. *Nat. Commun.* **2020**, *11*, 2451.
(22) Yue, L.; Gaarde, M. B. Introduction to theory of high-harmonic generation in solids: tutorial. *J. Opt. Soc. Am. B* **2022**, *39*, 535−555.
(23) El-Sherif; Briggs, N.; Bersch, B.; Pan, M.; Hamidinejad, M.; Rajabpour, S.; Filleter, T.; Kim, K. W.; Robinson, J. A.; Bassim, N. D. Scalable Characterization of 2D Gallium-Intercalated Epitaxial Graphene. *ACS Appl. Mater. Interfaces* **2021**, *13*, 55428−55439.
(24) Tamaya, T.; Ishikawa, A.; Ogawa, T.; Tanaka, K. Diabatic Mechanisms of Higher-Order Harmonic Generation in Solid-State Materials under High-Intensity Electric Fields. *Phys. Rev. Lett.* **2016**, *116*, No. 016601.
(25) Tamaya, T.; Ishikawa, A.; Ogawa, T.; Tanaka, K. Higher-order harmonic generation caused by elliptically polarized electric fields in solid-state materials. *Phys. Rev. B* **2016**, *94*, No. 241107.
(26) Novoselov, K. S.; Geim, A. K.; Morozov, S. V.; Jiang, D.; Katsnelson, M. I.; Grigorieva, I. V.; Dubonos, S. V.; Firsov, A. A. Two-dimensional gas of massless Dirac fermions in graphene. *Nature* **2005**, *438*, 197−200.
(27) Zhang, Y.; Tan, Y. W.; Stormer, H. L.; Kim, P. Experimental observation of the quantum Hall effect and Berry's phase in graphene. *Nature* **2005**, *438*, 201−204.
(28) Dietrich, P.; Burnett, N. H.; Ivanov, M.; Corkum, P. B. High-harmonic generation and correlated two-electron multiphoton ionization with elliptically polarized light. *Phys. Rev. A* **1994**, *50*, R3585.

https://doi.org/10.1021/acs.jpcc.4c08773
J. Phys. Chem. C 2025, 129, 5133−5139